Extreme Rainfall Events in the Hawaiian Islands

PAO-SHIN CHU

Department of Meteorology, School of Ocean and Earth Science and Technology, University of Hawaii at Manoa, Honolulu, Hawaii

XIN ZHAO

Department of Information and Computer Sciences, University of Hawaii at Manoa, Honolulu, Hawaii

YING RUAN AND MELODIE GRUBBS

Department of Meteorology, School of Ocean and Earth Science and Technology, University of Hawaii at Manoa, Honolulu, Hawaii

(Manuscript received 18 July 2007, in final form 29 July 2008)

ABSTRACT

Heavy rainfall and the associated floods occur frequently in the Hawaiian Islands and have caused huge economic losses as well as social problems. Extreme rainfall events in this study are defined by three different methods based on 1) the mean annual number of days on which 24-h accumulation exceeds a given daily rainfall amount, 2) the value associated with a specific daily rainfall percentile, and 3) the annual maximum daily rainfall values associated with a specific return period. For estimating the statistics of return periods, the three-parameter generalized extreme value distribution is fit using the method of L-moments. Spatial patterns of heavy and very heavy rainfall events across the islands are mapped separately based on the aforementioned three methods. Among all islands, the pattern on the island of Hawaii is most distinguishable, with a high frequency of events along the eastern slopes of Mauna Kea and a low frequency of events on the western portion so that a sharp gradient in extreme events from east to west is prominent. On other islands, extreme rainfall events tend to occur locally, mainly on the windward slopes. A case is presented for estimating return periods given different rainfall intensity for a station in Upper Manoa, Oahu. For the Halloween flood in 2004, the estimated return period is approximately 27 yr, and its true value should be no less than 13 yr with 95% confidence as determined from the adjusted bootstrap resampling technique.

1. Introduction

In the past few years, heavy rainfall events have resulted in major damage to properties, public infrastructure, agriculture, and tourism in the Hawaiian Islands. For example, torrential rainfall with 24-h totals as high as 940 mm (37 in.) caused flooding in the southeastern part of the island of Hawaii (Fig. 1) in early November 2000, with many homes damaged. Damage estimates reached about U.S. $88 million. In late October 2004, the upper Manoa Valley of Oahu received 254 mm (10 in.) of rainfall in a 12-h period, with a rainfall rate as high as 127 mm (5 in.) h^{-1}. Because Manoa Stream swelled and topped its banks, floodwater spilled onto residential areas and the University of Hawaii (UH) Manoa campus, with deposits of mud and debris. Estimates of damage for this flood are over US $80 million for UH alone. Heavy rainfall and flooding have also been frequently reported on other major islands such as Kauai and Maui (e.g., Lyman et al. 2005). In comparison with the mainland United States, extreme rainfall events in Hawaii have received little attention. Because of the socioeconomic repercussions of heavy rainfall and the associated floods on the islands, it is important to understand the frequency, intensity, locations, and patterns of these extreme events across the entire Hawaiian Islands. We thus propose to investigate the nature and spatial distributions of heavy and very heavy rainfall events in Hawaii.

Three different methods have commonly been used to identify extreme rainfall events. The first method is based on the actual rainfall amounts. Over the mainland United States, a ''heavy'' rainfall ''climatology'' is constructed on the basis of the mean annual number of days

Corresponding author address: Dr. Pao-Shin Chu, Department of Meteorology, 2525 Correa Rd., University of Hawaii at Manoa, Honolulu, HI 96822–2219.
E-mail: chu@hawaii.edu

DOI: 10.1175/2008JAMC1829.1

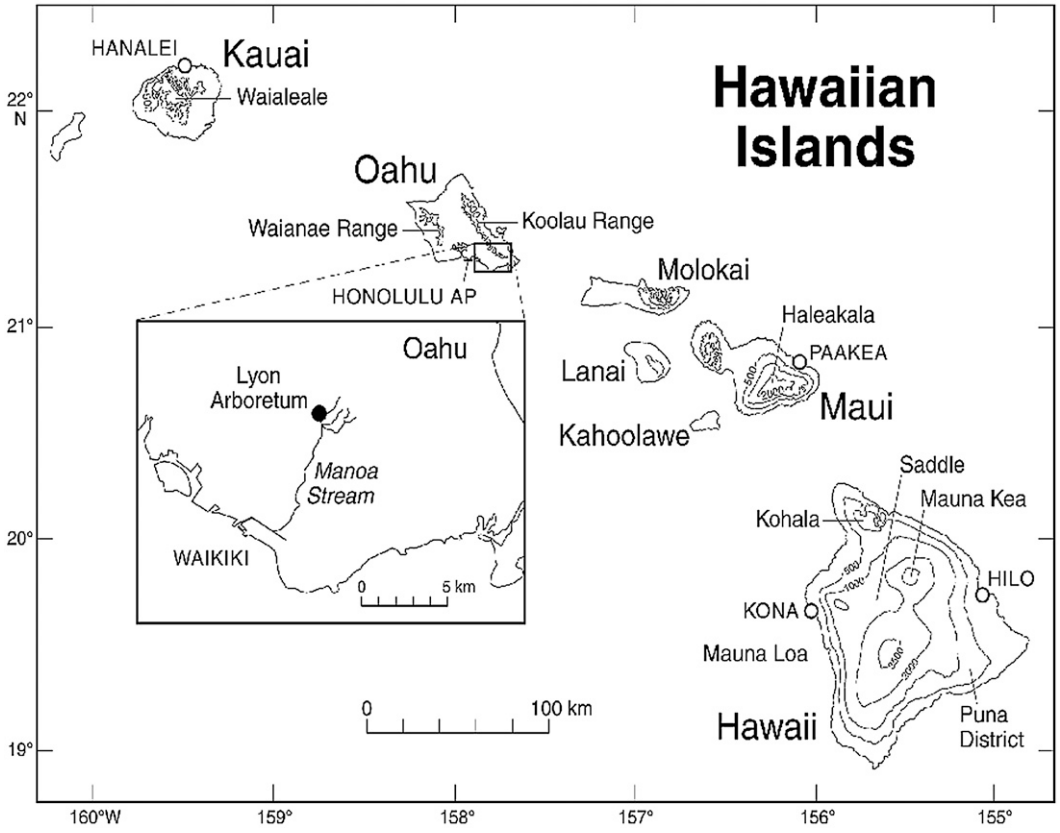

FIG. 1. Orientation map of the Hawaiian Islands, with contour intervals for elevation at 500, 1000, 2000, and 3000 m. The inset is for a portion of the island of Oahu.

on which 24-h accumulation exceeds 50.8 mm (2 in.) (Karl et al. 1996; Groisman et al. 1999). Likewise, a ''very heavy'' rainfall climatology is derived when daily precipitation exceeds 101.6 mm (4 in.). According to this definition, Groisman et al. (2001, hereinafter GKK01) showed that the maximum of heavy precipitation events is found in the Gulf States from Florida to Texas with an average of 4 days per year. The pattern of very heavy days is similar to that of the heavy precipitation days, although its spatial extent is more limited and the average number of events is reduced to no more than one event per year.

A second way to define extreme precipitation events is to use specific thresholds such as the 90th and 99th percentiles of precipitation days to define heavy and very heavy events, respectively (e.g., GKK01). Focusing on a very heavy case, a maximum value of more than 75 mm (2.95 in.) day^{-1} is located along a strip of the Gulf Coast in January, but of interest is that this maximum shifts northward toward the interior United States (e.g., Kansas and Oklahoma) in July (Fig. 1b in GKK01). This probably reflects the prevalence of summertime convective-type precipitation in the interior.

A third way of defining extreme precipitation events is to calculate return periods of the event based on the annual maximum 24-h precipitation series (e.g., Kunkel et al. 1999; GKK01). The largest single daily value in each of n years, known as the block maximum series, is chosen. Studies have shown that events that have a recurrence interval of 1 yr or longer have a high correlation with flooding in some regions of the United States (Changnon and Kunkel 1995). GKK01 produced maps for the return periods of 1 yr and 20 yr associated with maximum 24-h daily precipitation over the contiguous United States.

More than 45 years ago, the United States Weather Bureau (1962) published a report on recurrence intervals of rainfall intensity in Hawaii using records up to 1959. Subsequent to this report, rainfall frequency maps for Oahu using data up to 1981 were updated by Giambelluca et al. (1984). For both reports, the Gumbel distribution was employed to estimate the statistics of extreme values. Rainfall-frequency statistics are often used in determining peak discharges for streams, in the planning of flood hazards within watersheds, and in flood control systems (Lau and Mink 2006). Under the

scenario of doubled carbon dioxide, Zwiers and Kharin (1998) performed extreme-value analysis for daily precipitation at 10-, 20- and 50-yr return periods using simulated outputs from a general circulation model. In particular, they espoused the application of the generalized extreme value (GEV) distribution to the sample of annual extremes with the method of the L-moments. In this study, we also adopt the GEV model to analyze the annual maximum daily rainfall series for each station. Using a simple QQ-plot fit, we find that more than 95% variation (per R^2) of maximum daily rainfall series can be explained by the fitted GEV model for most stations.

The L-moments analysis has been used for determining regions of similar precipitation climates for the conterminous United States (Guttman 1993) and can be viewed as a modification of the probability-weighted moments (Hosking et al. 1985; Hosking and Wallis 1997). As compared with a regular moment estimator, L-moments statistics rely on ordered samples and yield fewer weights for extreme values. As a result, L-moments are usually more robust (or tolerant) to outliers than the moment method. Maximum likelihood (ML) estimation is another method often used to find distribution parameters that maximize the likelihood function. The ML method is an asymptotically unbiased (or consistent) estimator; however, it is not necessarily robust when the training sample size is limited or when outliers exist (Hosking et al. 1985). Martins and Stedinger (2000, 2001) more recently suggested a generalized maximum likelihood (GML) analysis method that imposes a prior distribution on the shape parameter of a GEV model so that the estimated shape parameter can be restricted to a reasonable range. Using several simulated examples, Martins and Stedinger demonstrated that the GML method marginally outperformed the L-moments method when the shape parameter of a GEV model is within the range $[-0.4, 0]$, whereas the L-moments method delivered relatively better results when the shape parameter is positive. Because there is no closed solution for estimating a GEV model using a GML method, an iterative method such as the Newton–Raphson algorithm is needed. In this study, we shall adopt the L-moments method to estimate GEV parameters because it often yields less bias than the method of maximum likelihood (Hosking and Wallis 1997; Zwiers and Kharin 1998) and is computationally easier than the GML.

As previously mentioned, a typical example of extreme-value data is the collection of annual maximum, or block maximum, daily precipitation values in each of n years. An alternative approach is to assemble the largest n values regardless of their year of occurrence. This approach is generally known as peaks-over-threshold (POT) or partial-duration data in hydrology because any values larger than a threshold are chosen. The advantage for the POT approach is that sample size is no longer limited to n in fitting a GEV model (Smith 1989). We admit that the POT approach and its associated generalized Pareto (GP) model are sound. However, selecting a proper threshold is still a critical problem in POT. In theory, this value has to be large enough to guarantee the exceedance convergence to a GP model. However, a value that is too high will noticeably decrease the sample size of the resulting partial-duration series, thus losing its edge over the corresponding GEV model. Selecting a relatively low threshold (Beguería and Vicente-Serrano 2006) downgrades the consistency of using a GP model and may lead to overfitting. Moreover, if the chosen threshold is small, the selected data under the POT approach may exhibit strong serial correlation, thus invalidating the theoretical probability distribution as a candidate model to describe the statistics of extremes (Wilks 2006). In this study, we use the GEV model and adopt an alternative approach to the data scarcity problem. To be specific, rather than trying to find a way to fit the data better, we attempt to provide an appropriate estimation with some confidence level for the uncertainty of the fitted GEV model parameters, along with the estimated quantiles for a given return period. The bootstrap method is a well-established Monte Carlo method used to estimate statistics for model parameters (Efron and Tibshirani 1993; Davison and Hinkley 1997; Chu and Wang 1998). Here, we design an adjusted bootstrap resampling procedure to give the confidence interval for the quantile estimation with the L-moments method as the core model parameter estimator.

The structure of this paper is as follows: Section 2 discusses the rainfall data used and the definition of extreme events. This is followed by section 3, in which we particularly address the GEV model, the way to use L-moments to estimate its associated model parameters, and how to find a lower bound for return periods with a given confidence level through a nonparametric adjusted bootstrap percentile procedure. Section 4 details the analysis results, and section 5 provides a summary and conclusions.

2. Data and data processing

The National Weather Service (NWS) cooperative stations provide the daily rainfall dataset (TD3200) used in this study (NCDC 2006). The station data can be obtained from the National Climatic Data Center (available online at (http://www.ncdc.noaa.gov/oa/ncdc.html).

A preliminary analysis of the TD3200[1] dataset reveals that there are 294 stations with daily rainfall records in the Hawaiian Islands. However, some gauges only have short records. To ensure statistical stability of the results, we opted to choose gauges with at least 20 yr of records with records up to 2005. In accord with these criteria, 158 stations were finally chosen.

Using the threshold of fixed 24-h rainfall amounts (i.e., the first definition), we identify the number of events for each year from each station. The mean annual number of days on which 24-h rainfall accumulation exceeds a threshold will subsequently be calculated. This will provide knowledge of the regions in which those events are most likely to occur and the frequency of their occurrences. Based on the chosen threshold of specific percentiles of the distribution for days with precipitation (the second definition), we will determine daily rainfall amounts of extreme events (i.e., the 90th and 99th percentiles). Here we ignore days of no precipitation or days with precipitation of less than 0.25 mm (0.01 in.). A third approach to define extreme events is to calculate the return period of daily rainfall from the sample of annual extremes exceeding some fixed high threshold; the return period, also called the recurrence interval, refers to the average period in which an event is expected to occur once in n years. We will produce maps for heavy and very heavy rainfall climatologies for two recurrence intervals (1 yr and 20 yr) separately using the three-parameter GEV distribution. To make the results robust, the method of L-moments is used to fit the GEV distribution to the samples of extremes.

3. Method: GEV distribution and its L-moment estimation

a. Return period and the GEV model

Let X be a random variable that only takes continuous real values. The cumulative distribution function (CDF) $F(x)$ and the probability density function (PDF) $f(x)$ of this variable are defined respectively as

$$F(x) = \Pr[X \le x] \quad \text{and} \quad f(x) = dF(x)/dx, \tag{1}$$

where the term $\Pr[A]$ denotes the probability of the event A. In many applications, a quantile is often expressed in terms of its "return period." The quantile of a return period T, denoted Q_T, is an event magnitude so extreme that it has probability $1/T$ of being exceeded by any single event. That is, for a given quantile value Q_T, its associated return period is

$$T = 1/[1 - F(Q_T)]. \tag{2}$$

The PDF and CDF of a GEV distribution are defined respectively by

$$f(x) = \alpha^{-1} \exp[-(1-\kappa)y - \exp(-y)] \quad \text{and} \tag{3a}$$

$$F(x) = \exp[-\exp(-y)], \tag{3b}$$

where

$$y = \begin{cases} -\dfrac{1}{\kappa}\log\left[1 - \dfrac{\kappa(x-\xi)}{\alpha}\right] & \kappa \neq 0 \\ \dfrac{x-\xi}{\alpha} & \kappa = 0 \end{cases} \quad \text{and}$$

$$\begin{aligned} -\infty < x \le \xi + \alpha/\kappa \quad & \kappa > 0 \\ -\infty < x < \infty \quad & \kappa = 0 \\ \xi + \alpha/\kappa \le x < \infty \quad & \kappa < 0 \end{aligned}$$

and the quantile function is

$$x = \begin{cases} \xi - \alpha \log[-\log(F)] & \kappa = 0 \\ \xi + \dfrac{\alpha}{\kappa}\{1 - [-\log(F)]^{\kappa}\} & \kappa \neq 0 \end{cases}. \tag{3c}$$

In a GEV distribution, there are three model parameters: the location parameter ξ, the scale parameter α, and the shape parameter κ. The commonly used two-parameter extreme value distributions, such as the Gumbel distribution (e.g., Chu and Wang 1998), is virtually a special case of the GEV distribution when $\kappa = 0$. The Gumbel distribution is known to underestimate large, infrequent rainfall events (Jenkinson 1955). The introduction of a shape parameter in a GEV distribution, in general, improves the fit to the upper tail (i.e., extremely large values).

b. Method of L-moments applied to the GEV model

In this study, GEV distribution parameters will be estimated by using the method of L-moments. L-moments fitting is often preferred for small data samples because it uses order statistics, and small sample size is often the case for rainfall records in the tropics.

When X has a GEV distribution, for $\kappa > -1$ the first three L-moments are defined as (Hosking and Wallis 1997)

$$\lambda_1 = \xi + (\alpha/\kappa)[1 - \Gamma(1+\kappa)],$$

$$\lambda_2 = (\alpha/\kappa)(1 - 2^{-\kappa})\Gamma(1+\kappa), \quad \text{and}$$

[1] The TD3200 dataset is composed primarily of stations in the NWS cooperative station network. This network includes the NWS principal climatological stations, volunteer observers, and stations from other federal agencies. The observing equipment used at all of these stations is calibrated and maintained by NWS field representatives, cooperative program managers, and hydrological/meteorological technicians.

$$\lambda_3 = \lambda_2\left[\frac{2(1-3^{-\kappa})}{1-2^{-\kappa}} - 3\right], \quad (4)$$

where $\Gamma()$ represents the gamma function:

$$\Gamma(x) = \int_0^\infty t^{x-1}e^{-t}\,dt, \quad x \geq 0.$$

In theory, all of the L-moments defined in (4) exist when $\kappa > -1$ and they uniquely determine the GEV distribution, but there is no explicit form to estimate the shape parameter κ. The following approximation given by Hosking et al. (1985), however, has an accuracy of better than 9×10^{-4} for $-0.5 \leq \lambda_3/\lambda_2 \leq 0.5$ (or, equivalent, $-0.46 \leq \kappa \leq 1.49$, which holds true for most real applications):

$$\kappa \approx 7.8590c + 2.9554c^2,$$

where

$$c = \frac{2}{3+\lambda_3/\lambda_2} - \frac{\log 2}{\log 3},$$

$$\alpha = \frac{\lambda_2\kappa}{(1-2^{-\kappa})\Gamma(1+\kappa)}, \quad \text{and}$$

$$\xi = \lambda_1 - (\alpha/\kappa)[1-\Gamma(1+\kappa)]. \quad (5)$$

A detailed discussion of the properties of L-moments can be found in Hosking and Wallis (1997). In practice, L-moments must be estimated from a finite number of samples. Let us assume that the sample size is N and that the samples are arranged in ascending order. That is,

$$\mathbf{X} = \{x_{1:N}, x_{2:N}, \ldots, x_{N:N} | x_{1:N} \leq x_{2:N} \leq \cdots \leq x_{N:N}\}.$$

The sample L-moments are thereby defined by

$$l_{r+1} = \sum_{k=0}^{r} P^*_{r,k} b_k, \quad r = 0, 1, \ldots, N-1,$$

where

$$P^*_{r,k} = (-1)^{r-k}\binom{r}{k}\binom{r+k}{k} = \frac{(-1)^{r-k}(r+k)!}{(k!)^2(r-k)!}, \quad k = 0, 1, \ldots, r, \quad \text{and}$$

$$b_r = \frac{1}{N}\binom{N-1}{r}^{-1}\sum_{j=r+1}^{N}\binom{j-1}{r}x_{j:N} = \frac{1}{N}\sum_{j=r+1}^{N}\frac{(j-1)(j-2)\cdots(j-r)}{(N-1)(N-2)\cdots(N-r)}x_{j:N}. \quad (6)$$

Sample L-moment l_r is an unbiased estimator of L-moment λ_r. In practice, to estimate all three model parameters of the GEV distribution with the given sorted samples $\mathbf{X}$ by using (5), one needs only to substitute the L-moments λ_r with the sample L-moments l_r using (6). With the estimated model parameters, one can calculate return period T for any given quantile (or rainfall intensity) Q_T with (2) and (3b). Note that we actually define 1-yr return period in this study as the case in which $T = 2$ in (2).

c. *Upper bound for quantile of a return period using an adjusted bootstrap method*

With the method described in sections 3a and 3b, one can easily calculate return period T for a target quantile Q_T and vice versa. However in many real applications, stakeholders also prefer to know how reliable the estimation of T or Q_T is. In other words, what is the lower (or conservative) bound of return period T for a given quantile Q_T or, the inverse, what is the upper bound of quantile Q_T for a given return period T, provided a 95% confidence interval? Instead of a simplified bootstrap procedure, we resort to a nonparametric adjusted bootstrap (BCa) method (Davison and Hinkley 1997) to estimate this value. This is justified because the distribution of estimation errors may not be symmetric, given the extreme quantiles used in this study. In the appendix, we show a detailed BCa procedure to estimate the upper bound of quantile Q_T for a given return period T. One can simulate a set of return-period values within a range of interest to get a comprehensive view of the upper bound of the quantile under a given α confidence level. The inverse function of this bound will be the lower bound of return period with respect to rainfall intensity.

4. Results

As described previously, extreme rainfall events in this study are defined by three different methods. The first two methods are derived from empirical quantiles of datasets and involve no fitting of theoretical probability distributions. They are described in sections 4a and 4b. The results in section 4c, based on the third method, are obtained by fitting a GEV distribution to annual daily maxima separately at each site.

A spatial analysis of the computed extreme statistics is conducted using proprietary geographic information system software (ArcGIS 9.0). The compiled statistics are plotted along with island coastlines. The spatial gradient is based on an inverse-distance-weighted interpolation algorithm. This simple scheme does not consider effects of complicated topographic or meteorological

(e.g., prevailing wind directions) features on rainfall extremes. In the areas where the spatial extent of the station network is sparse, caution should be exercised in the interpretation of the results. We have also tried the kriging method for spatial interpolation but results are monotonic and featureless in some cases. Therefore, only results based on an inverse-distance-weighted technique are presented.

a. Extreme events defined by specific rainfall amounts

1) HEAVY RAINFALL EVENTS

Figure 2a displays the heavy rainfall pattern as defined by the total number of days with more than 50.8 mm (2 in.) day^{-1} for all of the Hawaiian Islands. The most noteworthy feature is the relative maximum at a lower elevation on the eastern slopes of the islands for Hawaii, Maui, Oahu, and Kauai, with a maximum of 20–25 days throughout the year on the islands of Hawaii and Maui. As northeasterly trade winds from the open ocean are advected toward the islands, they are forced to rise along the windward slopes. This orographic uplift produces cooling, clouds, and rain. Moreover, thermally driven diurnal circulations such as land–sea breezes and mountain–valley winds also contribute to rainfall development by enhancing orographic uplifting of the trade winds and inducing low-level convergence with the trades (Leopold 1949; Garrett 1980; Chen and Nash 1994). As a result of thermal contrast between the elevated terrain and adjacent regions, daytime upslope, onshore flows and nighttime downslope, offshore flows develop along the eastern slope of the high mountains. Chen and Nash (1994) attributed the diurnal rainfall evolution to an interaction among orographic uplifting, thermal forcing, and the blocking of the trade winds by an island obstacle.

Because the orographic uplift is most pronounced below the trade-wind inversion, which usually occurs at a height of about 2000 m (Cao et al. 2007), high rainfall is commonly observed at lower elevations (approximately 600–1200 m) along the windward slope of the high mountains such as Mauna Kea and Mauna Loa, both of which exceed 4100 m in elevation (Fig. 1). As a consequence, the lower portion of the eastern flanks of Mauna Kea near Hilo is characterized by a maximum of heavy rainfall days (Fig. 2a), resulting from orographic rainfall caused by sea-breeze-aided trade winds. A small local maximum of 5–10 heavy rainfall days is found on the windward slope of Kohala in northern Hawaii. Of interest is that this is also the region where climatological mean annual rainfall exhibits a relative maximum due to the interaction of katabatic flows and trade winds rising up the Kohala mountain slopes.

In Fig. 2a, a band of heavy rainfall days (15–20 days) extending from the maximum in Hilo southward to Puna (Fig. 1) is noted. This region also coincides approximately with maximum climatological mean annual rainfall (Blumenstock and Price 1967; Giambelluca et al. 1986). As mentioned previously, orographic uplifting associated with onshore trade winds and thermal circulation on the heated slope during the day occurs in this region.

At high elevations well above the trade inversion that tends to suppress vertical lifting of air and thus convection, arid climate prevails. Being located in the lee of Mauna Kea and Mauna Loa, the western side of Hawaii is fairly dry (rain-shadow effect), with the mean annual rainfall being less than 508 mm (20 in) along the coast between Kohala and Kona. In Fig. 2a, central and west Hawaii are marked by a very low number of heavy rainfall days. Note also that although the island chain generally experiences winter rainy season and summer dry season, the Kona coast of Hawaii is unique in that more rainfall is observed in summer than in winter. This is caused by the daytime, onshore sea breeze that ascends the mountain slopes and interacts with the descending trade winds through the saddle (Fig. 1), producing local orographic showers in the late afternoon (Schroeder 1981). The sea-breeze circulation is more persistent in summer than in winter, leading to more rainfall in summer on the Kona coast. In the evening, the local circulation is dominated by katabatic land-breeze flow with few rainfall occurrences (Chen and Nash 1994). As such, the diurnal rainfall cycle is prominent and a unique summer rainfall maximum is present along the Kona coast. The high rainfall days on the east and low rainfall days on the west present an east-to-west rainfall-day gradient for the island of Hawaii (Fig. 2a).

For Maui, the eastern slope of Haleakala shows 5–10 heavy rainfall days, with a local maximum of 20–25 days at Paakea (Figs. 1 and 2a). The central valley and west Maui see a very low number of heavy rainfall days ($<$5 days). Two mean annual rainfall maxima occur on Maui—along the northeastern slope of Haleakala and at the summit of the west Maui mountains. The absence of a local maximum in heavy rainfall days near the summit of west Maui in Fig. 2a is attributed to the lack of rainfall stations in this study. Being located in the rain shadow of Maui and Molokai, Lanai is dry and, as a result, has a minimum of heavy rainfall days. Molokai also experiences a very low number of heavy rainfall days. However, there are only two stations available for Lanai and Molokai, and therefore the results may not be an accurate depiction of actual rainfall patterns there.

For Oahu, the windward side of the Ko′olau Range exhibits a maximum of 5–10 heavy rainfall days per year (Figs. 1 and 2a). Few heavy rainfall days are noted on

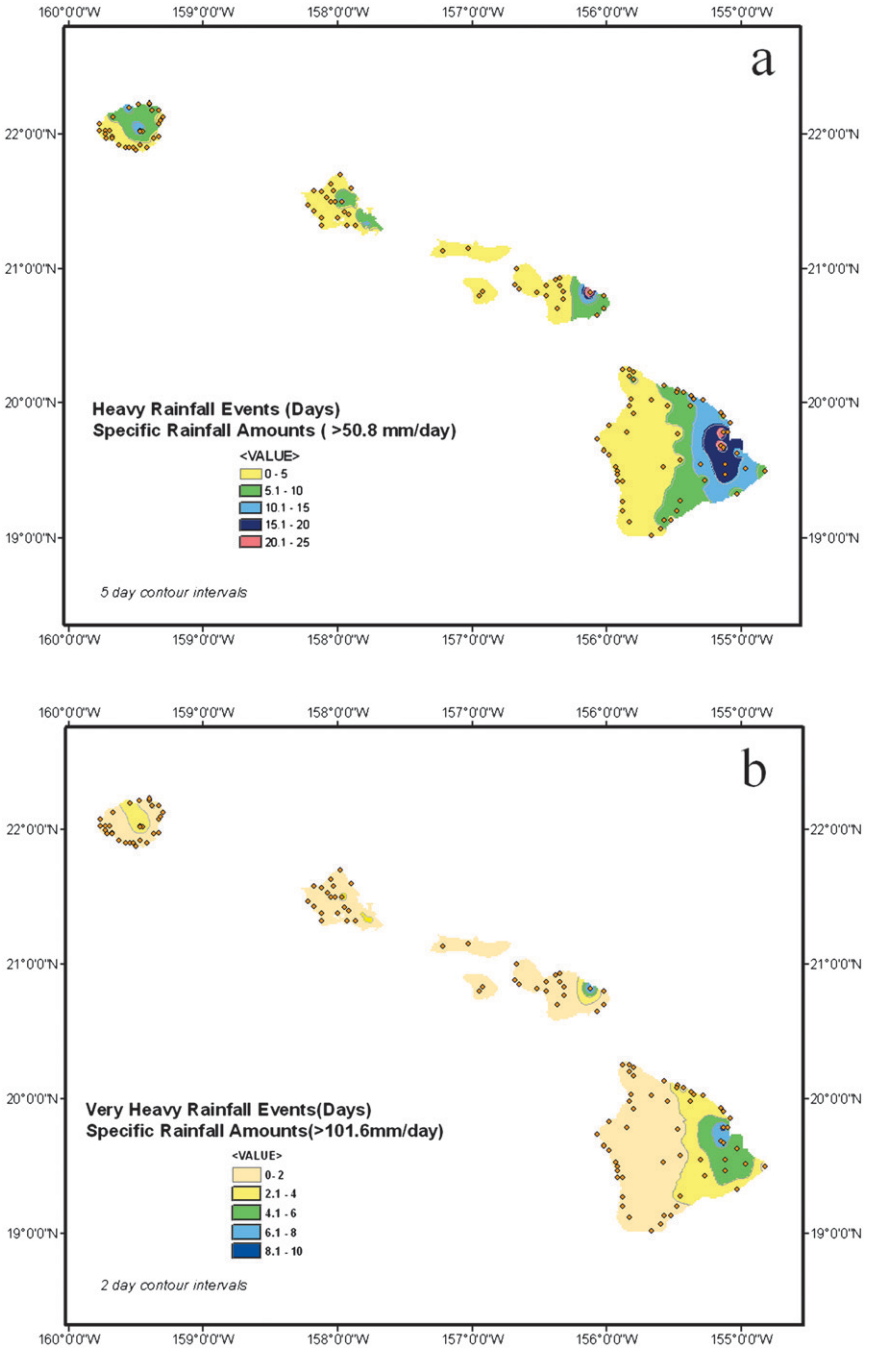

FIG. 2. (a) Spatial distribution (days) of heavy rainfall events defined by the mean annual number of days with 24-h rainfall accumulation above 50.8 mm (2 in.). (b) As in (a), but for very heavy rainfall events with 24-h rainfall above 101.6 mm (4 in.). Station locations are indicated except for those on east Oahu, which are shown in Fig. 5a.

west and north Oahu. The rest of the island experiences a low number of heavy rainfall events (0–5 days).

Kauai consists of one major volcanic mass with its highest elevation below the trade-wind inversion (Fig. 1). Thus, the north-facing slope is exposed to trade winds and is marked by a relative maximum of 5–10 heavy rainfall days (Fig. 2a). Because of its northernmost location, the island of Kauai experiences a few more cold-front storms of midlatitude nature than do the other Hawaiian islands. Also note a local maximum of 15–20

days near the central mountain summit of Waialeale at an elevation of 1597 m (Fig. 1). Because of the rounded shape of Kauai, its moderate-height volcano Waialeale is subject to wind and rain storms (e.g., Kona, upper-level trough) from any direction, and as a consequence this summit receives, on annual average, more than 10 160 mm (400 in.) of rain and is the wettest spot of all islands in Hawaii (Blumenstock and Price 1967). Kona storms are slow-moving, cutoff lows in the upper-level subtropical westerlies (Ramage 1962; Caruso and Businger 2006). During the cool season, they develop to the northwest of Hawaii with winds coming from the south or southwest persistently and are associated with surface lows. Kona lows last for days—some even more than a week—and may bring flooding to the islands. For a schematic model of Kona storms, see Chu et al. (1993).

2) VERY HEAVY RAINFALL EVENTS

The pattern of very heavy rainfall days is similar to that of heavy rainfall days, although the number of very heavy rainfall days is, of course, reduced relative to the heavy rainfall days (Figs. 2a,b). Again, the highest number of very heavy rainfall days (8–10 days) for the island of Hawaii is concentrated near Hilo and an east-to-west decrease in very heavy rainfall days is prominent for this island (Fig. 2b). Paakea on east Maui also experiences a large number of very heavy rainfall days (8–10 days). Oahu and Kauai are generally marked by <4 very heavy rainfall days.

b. Extreme events defined by specific percentiles of the distribution

1) HEAVY RAINFALL EVENTS

In Fig. 3a, the heavy rainfall patterns, represented by the 90th percentile of the daily rainfall distribution, exhibit features that are, to some extent, similar to those shown in Fig. 2a. For example, several spots with a local maximum of 40.1–50 mm day^{-1} are found on the eastern slope of Mauna Kea, and low daily rainfall values with 10.1–20 mm are seen on the westernmost part of the island of Hawaii (Fig. 3a). However, different from the corresponding previous map, the east-to-west gradient in rainfall amounts in Fig. 3a is not as pronounced as that in Fig. 2a. This is probably due to the different methods used for defining extreme events. For Maui (Fig. 3a), the windward slope near Paakea again shows a local maximum of 50.1–60 mm. For Oahu, most areas show low values except near the Ko‘olau summit and the westernmost tip of the island, where heavy rainfall with 20.1–30 mm day^{-1} is found (Fig. 3a). Kauai is marked by higher rainfall values (30.1–40 mm) scattered in several spots, including the central mountain summit.

2) VERY HEAVY RAINFALL EVENTS

For the very heavy rainfall events as denoted by the 99th percentile of the daily rainfall distribution (Fig. 3b), a maximum value with 220.1–240 mm is found near Hilo. The next highest amount, 180.1–200 mm, occurs on the southeastern slope of Mauna Loa. During the cool season, southeasterly winds may bring heavy rainfall to the southeastern slopes of Mauna Loa (e.g., Kodama and Barnes 1997). For example, on 2 November 2000, torrential rains with daily amounts as high as 759 mm (29.89 in.) were recorded at Kapapala Ranch (19°17′N, 155°27′W) in Pahala on the southeastern slope. A quasistationary upper-level low in the vicinity of Hawaii with an abundant moisture supply from Tropical Storm Paul to the east contributed to this storm event. The extraordinarily high rainfall fell at a single station, resulting in a bull’s-eye-shaped isolated maximum. Because the rainfall statistics presented in Fig. 3b are associated with the 99th percentile of the annual daily maximum rainfall, the largest value is simply not represented in Fig. 3b. Again, the western shores of this island exhibit a minimum of 40.1–60 mm, and an east–west asymmetry in rainfall amount is apparent. At the 99th percentile threshold, relative maxima of 80.1–100 mm prevail over Maui, Molokai, Lanai, Oahu, and Kauai. Again, even for dry western Oahu, 80.1–100 mm is not unexpected. Kauai is marked by higher rainfall amounts (100.1–120 mm) extending from the central mountain summit to the west and north.

c. Extreme events defined by return periods

1) HEAVY RAINFALL EVENTS

For the 1-yr return period (Fig. 4a), the eastern and southeastern slopes of the island of Hawaii experience a maximum of 200–250 mm daily rainfall; a decrease toward the west is found with a minimum of less than 100 mm on the western portion of the island. Even though a sea breeze circulation is prevalent in summer, it is not expected to bring heavy rainfall events in west Hawaii. For Maui, a single maximum of 200–250 mm day^{-1} is shown at Paakea and the 100–150-mm contour extends westward to the central upcountry. The overall pattern for Maui, Molokai, and Lanai in Fig. 4a is very similar to that exhibited according to the specific rainfall amounts (Fig. 2a). A large area with 100–150 mm of daily rainfall dominates over windward and central Oahu and a small area with 150–200 mm day^{-1} is found along the Ko‘olau Range of east Oahu (Fig. 4a). Areas that are expected to receive less than 100 mm of daily rainfall in any given year are the leeward coasts, including Honolulu International Airport, Ewa Beach, Kapolei, Makaha, and

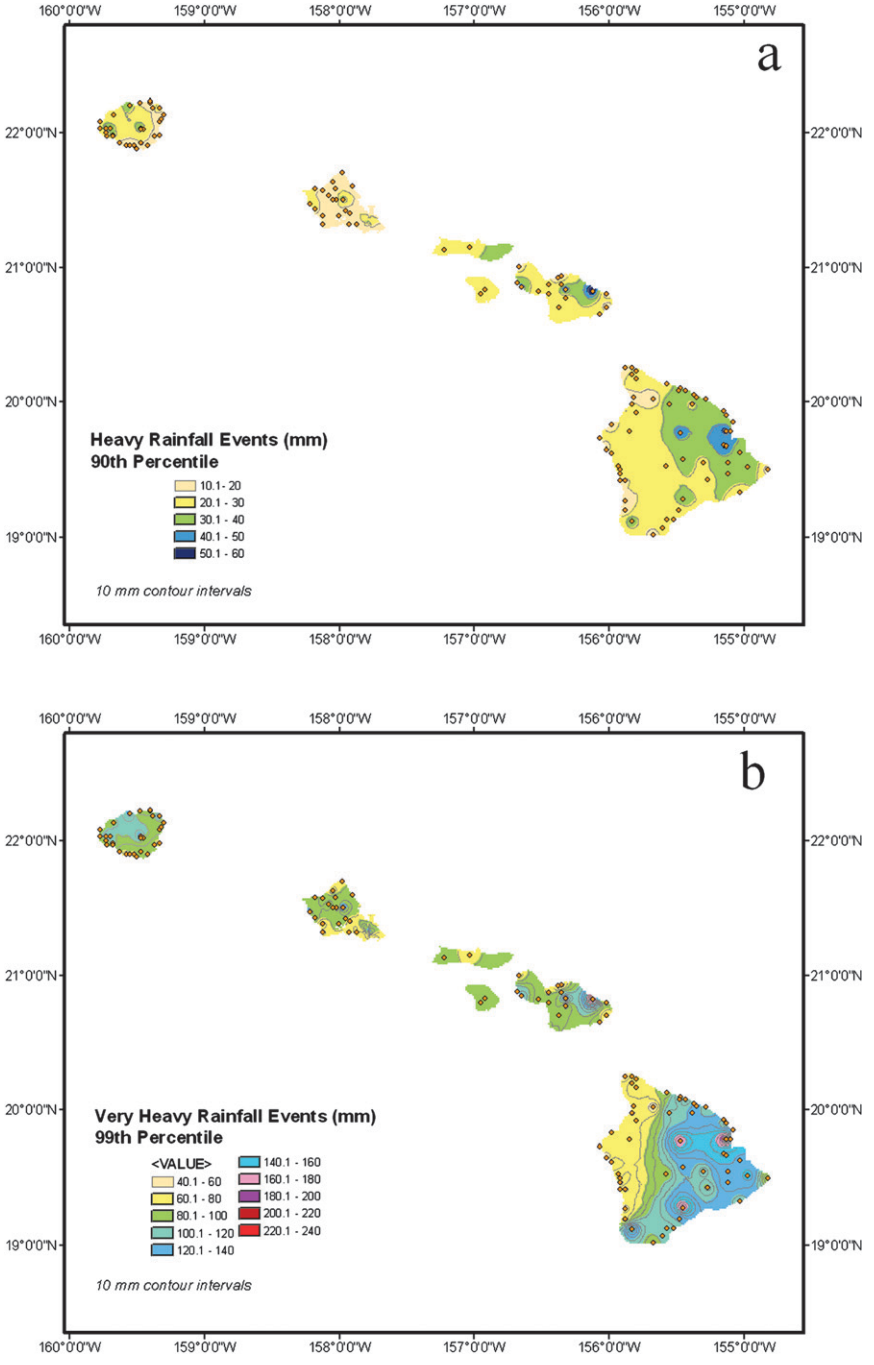

FIG. 3. (a) Spatial distribution (mm) of heavy rainfall events defined by the daily rainfall values associated with the 90th percentile of rainfall distribution in days with measurable rainfall. (b) As in (a), but for very heavy rainfall events with the 99th percentile of rainfall distribution.

Waianae. For Kauai (Fig. 4a), a band of maximum daily 150–200 mm extends from its central mountain summit northwestward to Hanalei and Princeville. Minimum values of less than 100 mm are found on the dry west shore.

2) VERY HEAVY RAINFALL EVENTS

For the 20-yr return period (Fig. 4b), the island of Hawaii sees several isolated spots of maxima with more than 400 mm day^{-1} near Hilo and higher than 500 mm day^{-1}

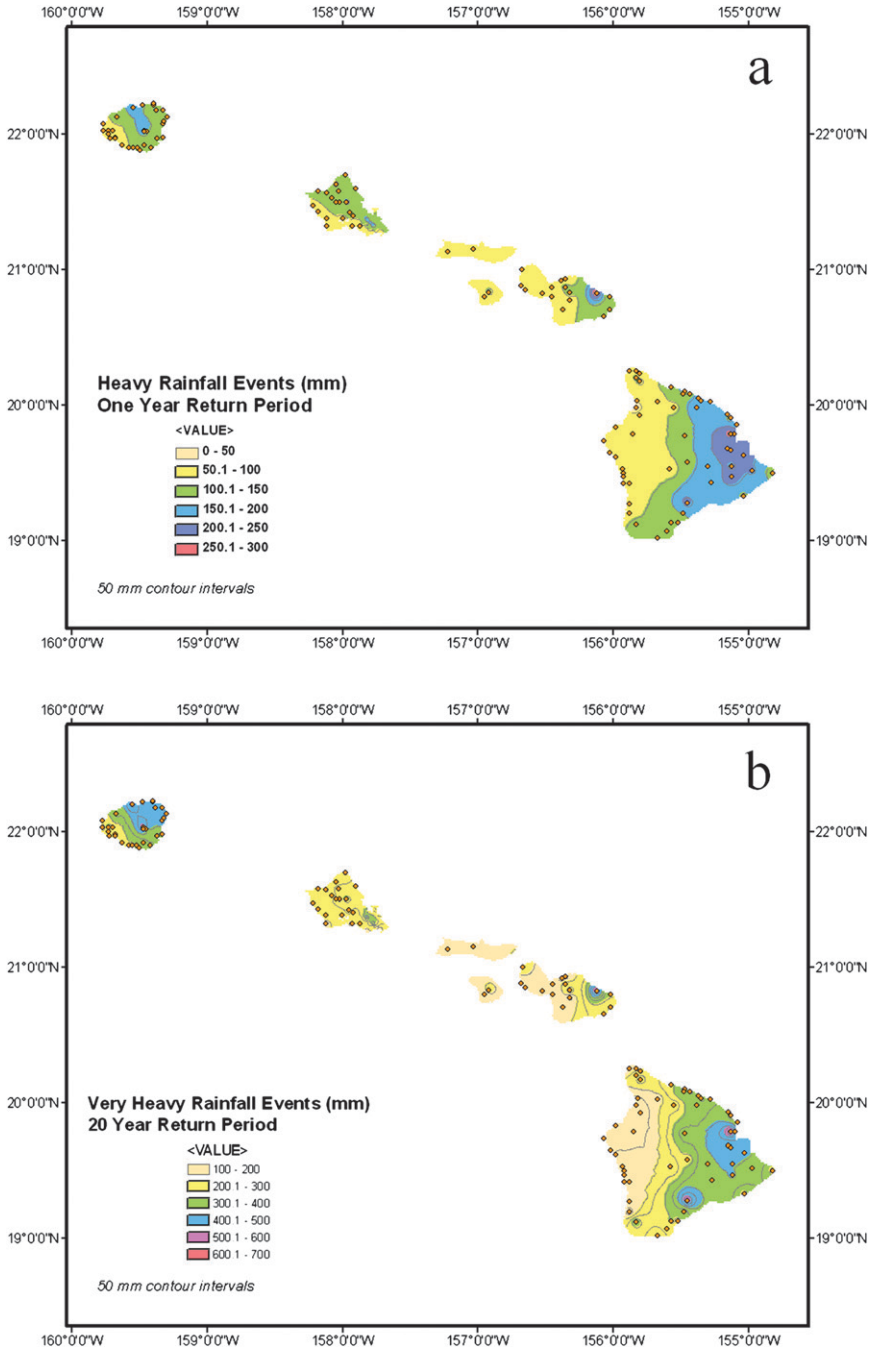

FIG. 4. (a) Spatial distribution (mm) of heavy rainfall events defined by 1-yr return values of the annual maximum daily rainfall using the GEV distribution. (b) As in (a), but for very heavy rainfall events defined by 20-yr return values.

at Kapapala Ranch (Fig. 1). Maui, like the island of Hawaii, shows an east–west asymmetry in extreme rainfall events at the 20-yr return period. For Oahu, because it is the most populated island in Hawaii, a separate and enlarged map is presented (Fig. 5a). With the exception of the leeward coast that includes Waikiki, Honolulu International Airport, and Kapolei, the daily maximum rainfall is more than 200 mm for almost the entire island. A band of maximum values of more than 300 mm day^{-1} is observed along the windward slope and the summit of Ko'olau Range in east Oahu from Kaneohe to Waimanalo. This maximum also extends slightly leeward of

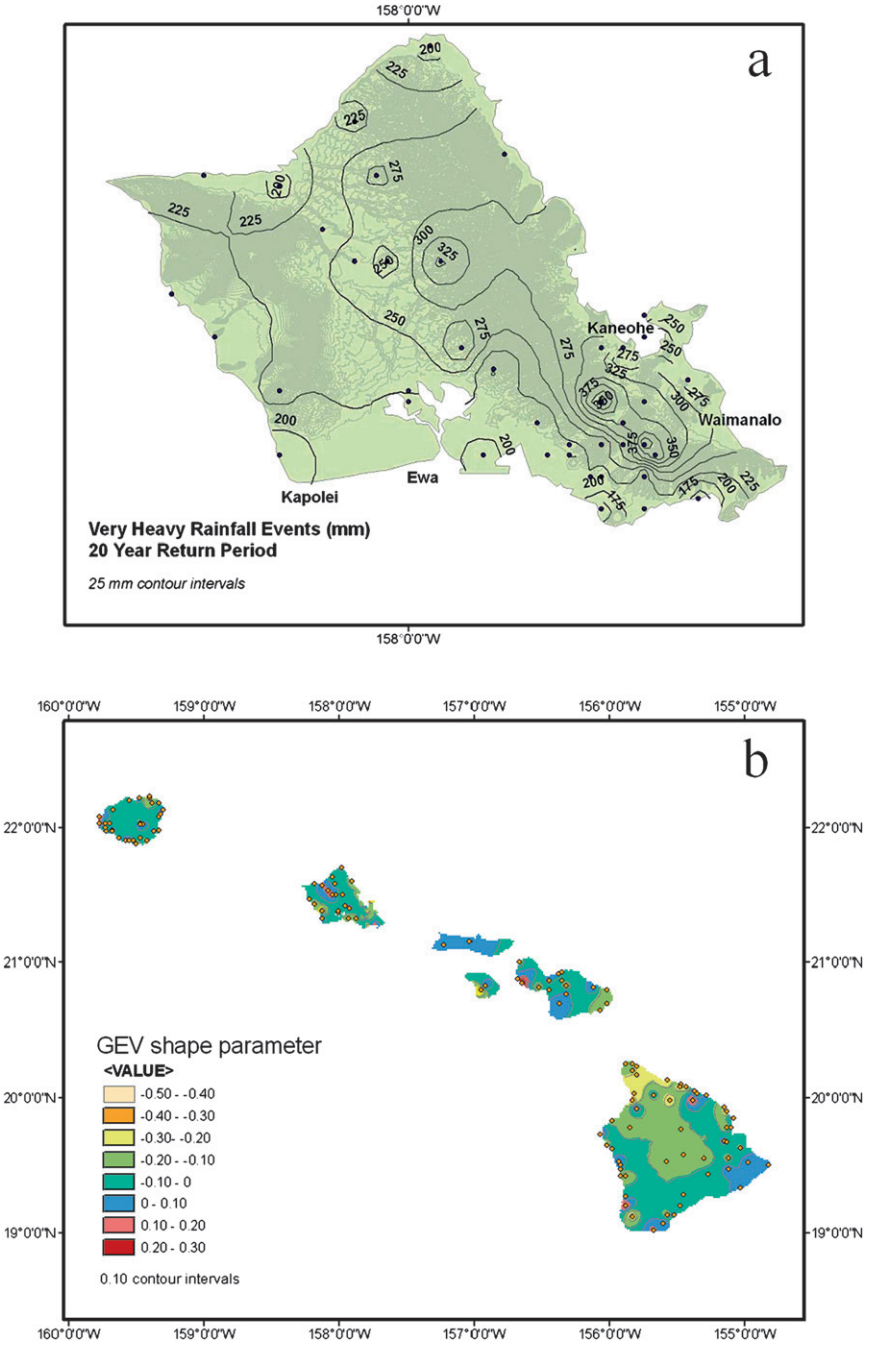

FIG. 5. (a) Spatial distribution of very heavy rainfall events based on return period for Oahu. Values are maximum daily rainfall (mm) associated with 20-yr recurrence intervals. (b) Spatial distribution of the GEV shape parameter. Station locations are indicated.

the summit, including upper Manoa and the adjacent Palolo Valley and Nuuanu. Because this is a 20-yr return period, the probability of observing this much daily rainfall in any single year is 5%.

Based on some NWS stations and other sources of gauges (e.g., the Honolulu Board of Water Supply), Giambelluca et al. (1984) produced various rainfall return period maps (e.g., 10- and 50-yr) for Oahu. For the daily records, the closest return period in Giambelluca et al. (1984) to our Fig. 5a is the 10-yr period. In their report, a maximum of 330 mm (13 in.) is found in east Oahu, almost in the same area as that in our Fig. 5a. Also

similarly to Fig. 5a, a minimum with less than 203 mm (8 in.) is found on the leeward coasts in Giambelluca et al. (1984). The major difference between Fig. 5a and Giambelluca et al. (1984) is the secondary maximum of more than 355 mm (14 in.) along the Ko'olau Range on northern Oahu in Giambelluca et al. (1984), whereas our analysis reveals only a local maximum of more than 300 mm in the same region. This difference may arise from the fact that our study, based entirely on the NWS cooperative stations (for reasons of being homogenous and quality controlled), is hampered by fewer gauges in mountainous regions. For Kauai (Fig. 4b), the northern portion of the island experiences 400–500 mm of daily rainfall, whereas the southwestern region is expected to receive less than 300 mm of rainfall for a 20-yr recurrence interval.

d. Spatial distribution of the GEV shape parameter

It is well known that the GEV distribution is reduced to a two-parameter Gumbel distribution when the shape parameter approaches zero. The GEV also incorporates two other special cases, a Frechet distribution for $\kappa < 0$ and a Weibull distribution for $\kappa > 0$. The more negative the shape parameter is, the longer (heavier) is its upper tail. Therefore, it is desirable to provide the information of the fitted shape parameter for the stations. Figure 5b displays the spatial distribution of the shape parameter for the Hawaiian Islands. Except for a few spots (e.g., Kohala, easternmost Maui), the shape parameter varies from -0.1 to 0.1 and is fairly close to zero. This suggests that the simple Gumbel distribution is a reasonable choice for most regions when the annual maximum daily rainfall series is used.

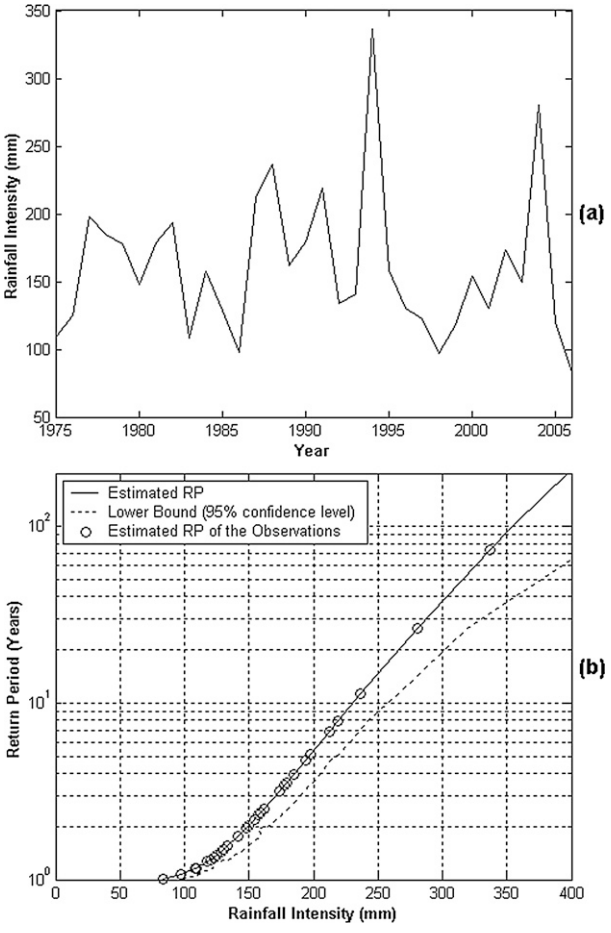

FIG. 6. (a) Time series of the annual maximum 24-h rainfall for Lyon Arboretum in Upper Manoa, Oahu; (b) the estimation of return periods of the annual maximum daily rainfall using the GEV distribution. The dashed line denotes the lower bound (i.e., conservative bound) of the estimate for the return period.

e. A case study of extreme events in upper Manoa, Oahu

As mentioned previously, the UH–Manoa campus suffered a major flood with substantial damage on 31 October 2004. Because of this disaster, it is of interest to investigate temporal variability of annual extremes and determine the return periods of this storm episode in the context of historical perspectives. Figure 6a shows the annual maximum series of daily rainfall at Lyon Arboretum in upper Manoa Valley, Oahu, from 1975 to 2006. Note that UH–Manoa is located immediately downstream from this locality (Fig. 1). Although a minimum value hovers around 100 mm day^{-1}, such as in 1986 and 1998, the annual maximum daily rainfall was as high as 336 mm in 1994, a factor of more than 3 to 1. This large variation seems to be consistent with the great variability of interannual rainfall found in the Hawaiian Islands (Chu 1995; Chu and Chen 2005). Figure 6b demonstrates the return periods of annual maximum daily rainfall at Lyon Arboretum for a range of rainfall intensity up to 400 mm. The three estimated GEV parameters are 5.31 (location), 1.51 (scale), and -0.094 (shape). The 95% confidence interval for the shape parameter is from -0.28 to 0.28. As seen in Fig. 6b, for the 20-yr return period, its relative rainfall intensity amount is 269 mm (10.6 in.). Because the observed annual maximum daily rainfall in 2004 is 280.7 mm (11.05 in.), its return period is greater than 20 yr (approximately 27 yr). The highest observed daily maximum rainfall is approximately 336 mm (observed in 1994), and its return period is 73 yr. For the 100-yr return period, the quantile of rainfall intensity is estimated to be 360 mm (14.2 in.).

We also plot the lower bound of the return period of its annual rainfall intensity (0–400 mm) with a 95% confidence level in Fig. 6b using the adjusted bootstrap

method. We applied the same procedure described in section 3c and performed 10 000 independent bootstrap samplings in the simulation. As a result, the dotted line in Fig. 6b demonstrates this lower bound of the return period. For the greatest daily rainfall ever recorded in upper Manoa in 1994 (corresponding to a maximum of 336 mm), its return period could be as small as 32 yr with this conservative measure. In other words, we are 95% certain that its return period cannot be smaller than 32 yr. For the Halloween flood in 2004, there is 95% certainty that its true return period should not be smaller than 13 yr.

5. Summary and conclusions

Assessing the vulnerability of a specific region to extreme rainfall and associated flood events is an important step in disaster prevention plans. Therefore, a climate risk assessment map involving heavy and very heavy rainfall events in the Hawaiian Islands is conducted using three different ways of defining extreme events. In specific terms, they are defined on the basis of the mean annual number of days on which 24-h rainfall accumulation exceeds a threshold, maximum daily rainfall associated with a specific percentile distribution, and annual maximum daily rainfall expected to occur once in a particular return period (using the generalized extreme value distribution, where distribution parameters are estimated using the L-moments). In this study, heavy (very heavy) rainfall events are those that exceed 50.8 (101.6) mm rainfall day^{-1}, are associated with the 90th (99th) percentile of daily rainfall distribution, and are associated with 1-yr (20 yr) return periods.

In particular, we implement the method of L-moments to estimate the return period for a given rainfall intensity with a GEV model and apply an adjusted bootstrap method to provide a lower bound for this statistic with a given confidence level. The method of L-moments is subject to fewer sampling fluctuations, and therefore the estimated distribution parameters are more robust than those determined from the conventional method of moment in which the skewness and kurtosis estimates are not known with good accuracy when the sample size is finite. The method of L-moments is also computationally simpler than both the maximum likelihood estimation and the generalized maximum likelihood methods. In the case study of the upper Manoa flood in Oahu, we show the details by applying the method described in section 3, and satisfactory results are achieved.

In a broad sense, risk event maps assembled from all three different methods yield qualitatively similar results, showing a concentration of extremely high rainfall events along the eastern slopes of the high mountains (e.g., Mauna Kea) and a low number of events in the leeward areas and atop the highest mountains. The extreme event pattern for the island of Kauai is somewhat different from those of the other major islands in that the northern coast as well as the Waialeale summit are subject to extremely high rainfall events. This is caused by a combination of several features: the round shape of the island, the moderate elevation of the summit, and the northernmost location of Kauai.

One cautionary note is that the results presented are based on the maximum rainfall that is accumulated for a fixed 24-h interval, usually beginning at 0000 UTC from a particular gauge. However, the true maximum 24-h rainfall event does not always fall in a fixed 24-h window. Rather, it may start at any time of the day and sometimes spans two consecutive days. In this regard, a moving window covering the true maximum 24-h event is more desirable. For practical reasons, this is not done in this study because the true-interval maximum is not observed by the standard gauges used here. Thus, the estimated rainfall associated with a specific return period in this study may be somewhat underestimated and needs to be multiplied by a factor of 1.143 (Weiss 1964) to approximate the true-interval observations. This is the approach adopted by Giambelluca et al. (1984).

The results presented here may benefit many local partners (e.g., state and county civil defense or state department of land and natural resources) who are concerned with floods and the relevant policy making. State agencies produced flood insurance rate maps in the 1970s. If the extreme rainfall statistics from the present study were to be merged with other geographic information system data layers (e.g., land use, historical flood damage in different zonings), then it would be possible to update the state flood insurance rate maps. In the future, we plan to work with state, county, and/or federal agencies to incorporate our current study into a more comprehensive analysis to better address the issue of economic damage caused by severe rainfall events in Hawaii.

Acknowledgments. This study was funded by the NOAA Pacific Region Integrated Data Enterprise (PRIDE) project and NOAA/NCDC through JIMAR to the University of Hawaii. Constructive criticisms from three anonymous reviewers helped greatly to improve the presentation of this paper. Thanks are also given to Kevin Kodama for the monthly precipitation summary, Cheryl Anderson for suggestions on the state hazard mitigation planning, Howard Diamond for references on NOAA Cooperative Stations, Editor Dr. Julie Winkler for handling the paper, and Di Henderson for technical editing.

APPENDIX

A Nonparametric Adjusted Bootstrap Method

Bootstrapping is a simple but powerful Monte Carlo method to assess statistical accuracy or to estimate the distribution of sample statistics. As long as the training samples are valid representatives of the analyzed population, the bootstrap method provides legitimate information for the model parameters. Suppose there are N training samples, and for each simulation we draw L independent bootstrap samplings. Within each bootstrap sampling, we independently draw N samples with replacement from the pool of training samples. Through the procedure shown in sections 3a and 3b, we estimate the quantile Q_T with respect to the target return period T based on the resampled dataset within each iteration. After L bootstrap iterations, in the end, for the target return period T, we obtain L estimations of the quantile. We then sort this estimated quantile set in an ascending order and denote it by $\mathbf{Q}_T^* = \{Q_{T1}^*, \ldots, Q_{TL}^* | Q_1^* \leq \cdots \leq Q_{TL}^*\}$. If the confidence level for the bound is α, the BCa procedure to get the upper (conservative) bound for the quantile Q_T is described in the following. [Refer to Davison and Hinkley (1997) for the technical details and mathematical derivations of a BCa method.]

We first calculate the empirical influence values of the observation set, which for a quantile estimator can be formulated by

$$\mathrm{EIV}_i = \begin{cases} \dfrac{F(Q_T) - 1}{f(Q_T)}, & X_i \leq Q_T \\ \dfrac{F(Q_T)}{f(Q_T)}, & X_i > Q_T \end{cases} \quad \text{for } i = 1, 2, \ldots, N. \tag{A1}$$

In (A1), the cumulative function $F()$ and density function $f()$ are referring to the fitted GEV distribution model with the parameters estimated by applying the L-moments method described in sections 3a and 3b to the real observation set. With the estimated quantile set $\mathbf{Q}_T^* = \{Q_{T1}^*, \ldots, Q_{TL}^* | Q_1^* \leq \cdots \leq Q_{TL}^*\}$, the upper bound limit for Q_T with α confidence level can be expressed in terms of simulation values:

$$\hat{Q}_T(\alpha) = Q_{T,(L+1)\tilde{\alpha}}^*, \tag{A2}$$

where

$$\tilde{\alpha} = \Phi\left[w + \frac{w + z_{\alpha'}}{1 - a(w + z_{\alpha'})}\right],$$

$$\Phi(x) = \int_{-\infty}^{x} (2\pi)^{-1/2} \exp(-x^2/2)\, dx,$$

$$z_{\alpha'} = \Phi(\alpha'), \quad \text{and}$$

$$\alpha' = 1 - \alpha.$$

In (A2), Φ is the cumulative distribution function of the standard normal distribution and the parameter a is calculated by

$$a = \frac{1}{6} \frac{\sum_{i=1}^{N} \mathrm{EIV}_i^3}{\left(\sum_{i=1}^{N} \mathrm{EIV}_i^2\right)^{3/2}} \quad \text{for } i = 1, 2, \ldots, N, \tag{A3}$$

where EIV_i is defined in (A1). The parameter w in (A2) can be estimated by

$$w = \Phi^{-1}\left(\frac{\#\{Q_{Tr}^* \leq Q_T | r = 1, \ldots, L\}}{L + 1}\right). \tag{A4}$$

In (A4), quantile Q_T is the same as defined in (A1); function $\#\{Q_{Tr}^* \leq Q_T | r = 1, \ldots, L\}$ represents the number of elements in set $\mathbf{Q}_T^*$ that are smaller than or equal to Q_T, and function Φ^{-1} denotes the inverse function of the function Φ defined in (A2).

In (A2), the subscript index $(L + 1)\tilde{\alpha}$ usually is not an integer. Therefore, the following interpolation procedure should be applied to calculate the bound $\hat{Q}_T(\alpha)$:

$$Q_{T,(L+1)\tilde{\alpha}}^* = Q_{T,k}^* + \frac{\Phi^{-1}(\tilde{\alpha}) - \Phi^{-1}\left(\dfrac{k}{L+1}\right)}{\Phi^{-1}\left(\dfrac{k+1}{L+1}\right) - \Phi^{-1}\left(\dfrac{k}{L+1}\right)} \times (Q_{T,k+1}^* - Q_{T,k}^*), \tag{A5}$$

where k is the integer part of the value $(L + 1)\tilde{\alpha}$.

REFERENCES

Beguería, S., and S. M. Vicente-Serrano, 2006: Mapping the hazard of extreme rainfall by peaks over threshold extreme value analysis and spatial regression techniques. *J. Appl. Meteor. Climatol.,* **45,** 108–124.

Blumenstock, D., and S. Price, 1967: Hawaii. Climates of the States Series, U.S. Weather Bureau, 27 pp.

Cao, G., T. W. Giambelluca, D. E. Stevens, and T. A. Schroeder, 2007: Inversion variability in the Hawaiian trade wind regime. *J. Climate,* **20,** 1145–1160.

Caruso, S. J., and S. Businger, 2006: Subtropical cyclogenesis over the central North Pacific. *Wea. Forecasting,* **21,** 193–205.

Changnon, S. A., and K. E. Kunkel, 1995: Climate-related fluctuations in Midwestern flooding. *J. Water Resour. Plann. Manage.,* **121,** 326–334.

Chen, Y.-L., and A. J. Nash, 1994: Diurnal variation of surface airflow and rainfall frequencies on the island of Hawaii. *Mon. Wea. Rev.,* **122,** 34–56.

Chu, P.-S., 1995: Hawaii rainfall anomalies and El Niño. *J. Climate,* **8,** 1697–1703.

——, and J. Wang, 1998: Modeling return periods of tropical cyclone intensities in the vicinity of Hawaii. *J. Appl. Meteor.,* **37,** 951–960.

——, and H. Chen, 2005: Interannual and interdecadal rainfall variations in the Hawaiian Islands. *J. Climate,* **18,** 4796–4813.

——, A. J. Nash, and F. Porter, 1993: Diagnostic studies of two contrasting rainfall episodes in Hawaii: Dry 1981 and wet 1982. *J. Climate,* **6,** 1457–1462.

Davison, A. C., and D. V. Hinkley, 1997: *Bootstrap Methods and Their Applications*. Cambridge University Press, 582 pp.

Efron, B., and R. J. Tibshirani, 1993: *An Introduction to the Bootstrap*. Chapman and Hall, 436 pp.

Garrett, A. J., 1980: Orographic cloud over the eastern slopes of Mauna Loa volcano, Hawaii, related to insolation and wind. *Mon. Wea. Rev.,* **108,** 931–941.

Giambelluca, T. W., L. S. Lau, Y. S. Fok, and T. A. Schroeder, 1984: Rainfall frequency study for Oahu. State of Hawaii Department of Land and Natural Resources Rep. R73, 34 pp.

——, M. A. Nullet, and T. A. Schroeder, 1986: Rainfall atlas of Hawai'i. State of Hawaii Department of Land and Natural Resources Rep. R76, 267 pp.

Groisman, P. Ya., and Coauthors, 1999: Changes in the probability of heavy precipitation: Important indicators of climatic change. *Climatic Change,* **42,** 243–283.

——, R. W. Knight, and T. R. Karl, 2001: Heavy precipitation and high streamflow in the contiguous United States: Trends in the twentieth century. *Bull. Amer. Meteor. Soc.,* **82,** 219–246.

Guttman, N. B., 1993: The use of L-moments in the determination of regional precipitation climates. *J. Climate,* **6,** 2309–2325.

Hosking, J. R. M., and J. R. Wallis, 1997: *Regional Frequency Analysis: An Approach Based on L-Moments*. Cambridge University Press, 224 pp.

——, ——, and E. F. Wood, 1985: Estimation of the generalized extreme-value distribution by the method of probability-weighted moments. *Technometrics,* **27,** 251–261.

Jenkinson, A. F., 1955: The frequency distribution of the annual maximum (or minimum) values of meteorological elements. *Quart. J. Roy. Meteor. Soc.,* **81,** 158–171.

Karl, T. R., R. W. Knight, D. R. Easterling, and R. G. Quayle, 1996: Indices of climate change for the United States. *Bull. Amer. Meteor. Soc.,* **77,** 279–292.

Kodama, K., and G. M. Barnes, 1997: Heavy rain events over the south-facing slopes of Hawaii: Attendant conditions. *Wea. Forecasting,* **12,** 347–367.

Kunkel, K. E., K. Andsager, and D. R. Easterling, 1999: Long-term trends in extreme precipitation events over the conterminous United States and Canada. *J. Climate,* **12,** 2515–2527.

Lau, L. S., and J. F. Mink, 2006: *Hydrology of the Hawaiian Islands*. University of Hawaii Press, 274 pp.

Leopold, L. B., 1949: The interaction of trade wind and sea breeze, Hawaii. *J. Meteor.,* **6,** 312–320.

Lyman, R. E., T. A. Schroeder, and G. M. Barnes, 2005: The heavy rain event of 29 October 2000 in Hana, Maui. *Wea. Forecasting,* **20,** 397–414.

Martins, E. S., and J. R. Stedinger, 2000: Generalized maximum-likelihood generalized extreme-value quantile estimators for hydrologic data. *Water Resour. Res.,* **36,** 737–744.

——, and ——, 2001: Generalized maximum likelihood Pareto–Poisson estimators for partial duration series. *Water Resour. Res.,* **37,** 2551–2557.

NCDC, 2006: Data documentation for data set 3200 (DSI-3200), surface land daily cooperative summary of the day. National Climatic Data Center, 19 pp.

Ramage, C. S., 1962: The subtropical cyclone. *J. Geophys. Res.,* **67,** 1401–1411.

Schroeder, T. A., 1981: Characteristics of local winds in northwest Hawaii. *J. Appl. Meteor.,* **20,** 874–881.

Smith, R. L., 1989: Extreme value analysis of environmental time series: An application to trend detection in ground-level ozone. *Stat. Sci.,* **4,** 367–377.

United States Weather Bureau, 1962: Rainfall-frequency atlas for the Hawaiian Islands for areas to 200 square miles, duration to 24 hours, and return periods from 1 to 100 years. Weather Bureau Tech. Paper 43, 60 pp.

Weiss, L. L., 1964: Ratio of true to fixed interval maximum rainfall. *J. Hydraul. Div., Amer. Soc. Civ. Eng.,* **90,** 77–82.

Wilks, D. S., 2006: *Statistical Methods in the Atmospheric Sciences*. 2nd ed. Academic Press, 627 pp.

Zwiers, F. W., and V. V. Kharin, 1998: Changes in the extremes of the climate simulated by CCC GCM2 under CO_2 doubling. *J. Climate,* **11,** 2200–2222.